

Multipath and Attitude Estimation Phase Lock Loop for Antenna Array Signal Processing

Daniel S. Maier, *Universität der Bundeswehr München*
Thomas Pany, *Universität der Bundeswehr München*

BIOGRAPHY (IES)

Daniel S. Maier received a bachelor in Physics in 2015 and a master in Applied and Engineering Physics in 2017 from the Technical University of Munich (TUM), Germany. Since 2017 he has been a research associate at the Institute of Space Technology and Space Applications of the “Universität der Bundeswehr München.” His current research interests include GNSS signal generation, signal authentication, and signal performance analysis.

Prof. Thomas Pany is with the Universität der Bundeswehr München at Space Systems Research Center (FZ-Space) where he leads the satellite navigation unit LRT 9.2 of the Institute of Space Technology and Space Applications (ISTA). He teaches navigation focusing on GNSS, sensors fusion and aerospace applications. Within LRT 9.2 a good dozen of full-time researchers investigate GNSS system and signal design, GNSS transceivers and high-integrity multi-sensor navigation (inertial, LiDAR) and is also developing a modular UAV-based GNSS test bed. ISTA also develops the MuSNAT GNSS software receiver and recently focuses on smartphone positioning and GNSS/5G integration. He has a PhD from the Graz University of Technology (sub auspiciis) and worked in the GNSS industry for seven years. He authored around 200 publications including one monography and received five best presentation awards from the US Institute of Navigation.

ABSTRACT

This work presents a new GNSS array processing algorithm to estimate simultaneously the antenna array attitude and the direction of incoming multipath wave fronts. The **multipath and attitude estimating phase lock loop (MAEPLL)** is a post-correlation technique based on the parallel processing of the prompt correlator values from the antenna elements, forming double-differenced prompt correlator (DDPC) values between antenna elements and satellites. With a geometrical based model of the derived DDPC values the attitude and the multipath direction of arrival (DOA) can be estimated. Non-adaptive beamforming techniques can use the estimated platform attitude and multipath DOA to obtain conventional (not differenced) correlation values. With classical DLL/FLL/PLL filters the position, velocity and timing (PVT) solution is derived after the beamforming process. On the basis of a self-developed wideband multipath channel simulation framework we present our first results for the attitude and multipath DOA estimation accuracy. The results show, that the attitude accuracy is quite independent of the environmental conditions due to the double-differencing. It is also shown, that it is possible to jointly estimate antenna array attitude and multipath direction of arrival. This work outlines the mathematical foundations of a combined multipath and attitude estimation based on DDPC values. The simulation results show attitude accuracies below one degree in all three spatial directions, as well as high robustness in terms of initially assumed attitudes, multipath environments and signal strengths. The MAEPLL technique has the potential to extend the DDPC model to include an estimation of the antenna element phase center corrections (PCCs), enabling the use of cheap, sub-optimal, uncalibrated and integrated antenna arrays in mass-market applications with on-the-fly antenna phase center variation calibration.

INTRODUCTION

Future trends like autonomous driving, urban air mobility, augmented reality (AR), internet of things (IoT) and asset tracking bring new challenges and requirements to the global navigation satellite system (GNSS). Many of the new applications will be deployed in suburban, urban and densely populated areas, where they must operate reliably. Apart from the challenging environment with signal blocking, strong multipath conditions and potential radio-frequency interferences (RFI) these applications require the positioning solutions to be with in an accuracy in the centimeter range, with high confidence and high security levels to enable safety-of-life critical applications like autonomous driving. Under these conditions, the usage of antenna arrays can help significantly to achieve the requirements as antenna arrays provide spatial measures to increase the signal-to-noise-plus-interference ratio (SINR) applying beamforming in line of sight (LOS) direction and nulling to tackle multipath and interference (RFI,

Jamming and Spoofing) related issues. However, this is only possible if the drawbacks of antenna array systems namely bulky size, high costs and the need for calibration can be tackled and allow the usage in mass-market applications. The usage of antenna arrays can also improve the situation regarding the multipath degradation if the array attitude is known and the multipath direction can be estimated.

The basic processing techniques and configurations of antenna arrays are, as well as RTK, well studied and explained in the literature e.g. [1]. There are also studies using antenna arrays for GNSS applications. The main applications of antenna arrays in GNSS are on the one hand the detection and mitigation of interference, being commonly done in a pre-correlation process. The interference detection with antenna array is based on the fact that the GNSS signals are below the noise floor and interfering signals being above the noise floor. With a spatial analysis of the raw samples of the antenna elements and their variances it is possible to detect the direction of arrival (DOA) of the interference and is cancelled with a Null-steering of the antenna array [2]. On the other hand, the beamforming is used in a post-correlation step to increase the SNR of the satellite signals and to reduce the influence of multipath signals. This is possible because the DOA of the satellite signals are known from the almanac. It is also possible to detect spoofing signals when they arrive from wrong DOA, see [3] and [4]. A block diagram for pre- and post-correlation is shown in Figure 1 adopted from [5] where pre- and post-correlation techniques in GNSS are well explained. With uncalibrated sub-optimal antenna arrays it is still possible to use pre-correlation filter for interference mitigation which rely on the covariance matrix. Non-adaptive Beamforming, however, is not possible with sub-optimal antenna arrays. For calculating the DOA of the incoming signal from time delays or phase shifts it is necessary to have full knowledge of phase center offsets, phase delays, hardware delays and crosstalk effects of the antenna elements in the array. Studies have shown that it is possible to use GNSS live signals to calibrate the multi-antenna array on the fly [6], where additionally the attitude of the antenna array is estimated [7]. In the work of [8] the antenna attitude, the spoofing and jamming detection and the mitigation as well as the calibration is treated as a coupled problem, where the unknowns are estimated together.

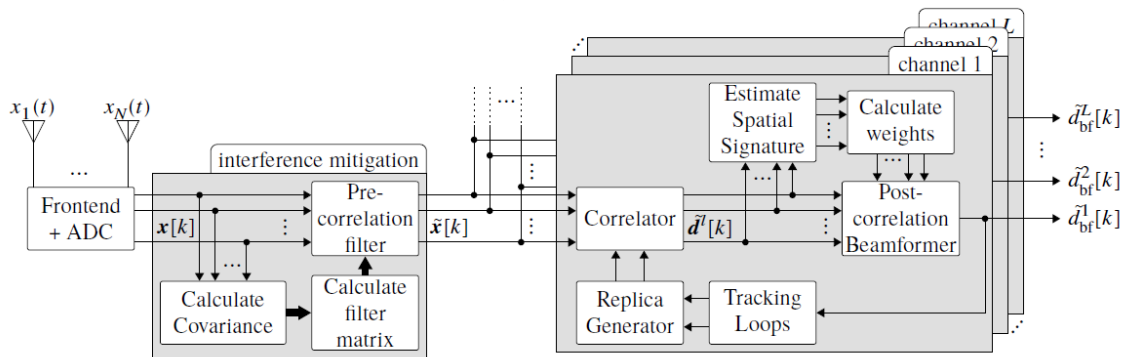


Figure 1. Block diagram for Null-steering and Beamforming in pre- and post-correlation. [5]

MAEPLL CONCEPT

MAEPLL is meant to be integrated into a closed vector tracking loop with an integrated extended Kalman-Filter (EKF). The MAEPLL processing includes the MAEPLL core and the beamforming, see Figure 2. In the MAEPLL core the double-differenced prompt correlator (DDPC) values are used to estimate the platform attitude and the DOA of the multipath (MP) wave fronts. The beamforming stage applies a non-adaptive beamforming algorithm to enhance the LOS signal and suppress the MP components. Non-adaptive beamforming refers to the circumstance that the array steering vector is only set accordingly to the geometrical conditions. After the beamforming (combination of prompt correlator values of the antenna elements), the enhanced correlator outputs are used in classical DLL/FLL/PLL filters. The estimation of position, velocity and timing (PVT) can be performed using well-known positioning techniques like SPP, RTK or PPP. Further, it is assumed that the rough receiver position and the satellite almanac are known. The approximated attitude is also known from IMU measurements (cheap IMU) or previous update steps of the EKF. In Figure 2 the block diagram of the MAEPLL receiver architecture is sketched, where the red area indicates the core of the MAEPLL technique. In this paper only the MAEPLL core functionality is studied, the other parts are assumed to work as intended. Also, all received signals from all antenna elements are tracked on a common NCO basis (slaved tracking) and are combined in the double-differenced prompt correlator values used for the following estimation process. The double-differencing, between the antenna array elements and the satellites in view, of the complex prompt correlator outputs allow an easy access on array attitude, array

geometry and multipath conditions. Dual- or multi-frequency signal processing is used to strengthen the combined estimation process of multipath DOA, platform attitude and array geometry.

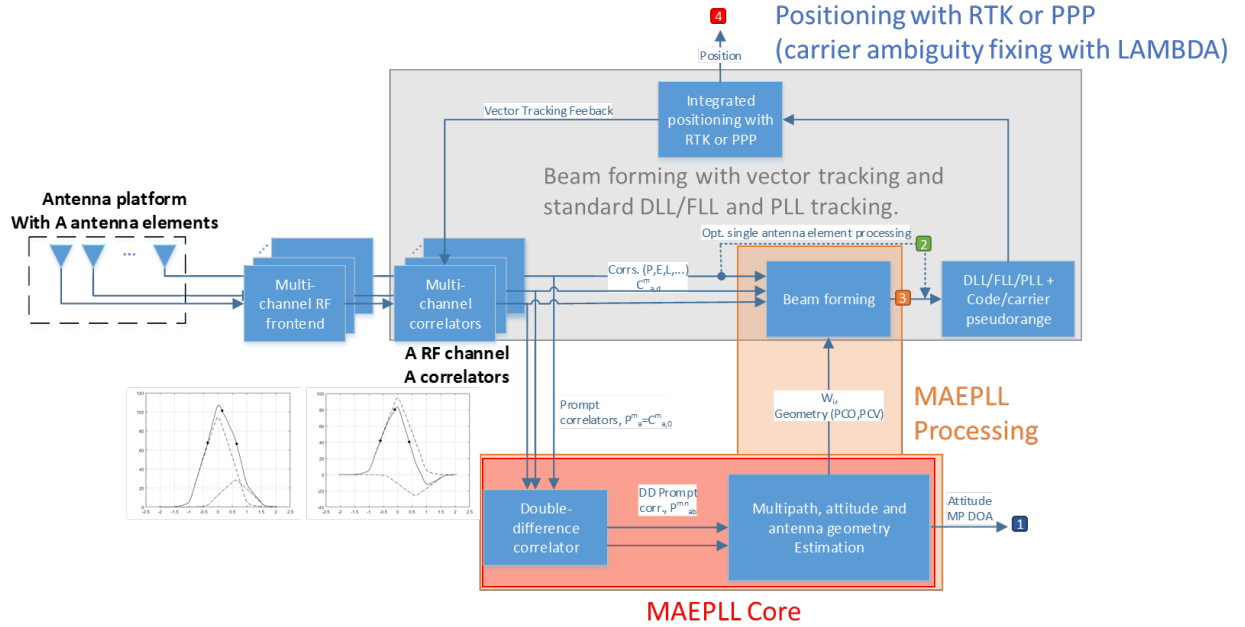


Figure 2: Block diagram of a multi-antenna, post-correlation beamforming, vector tracking and positioning approach. The antenna attitude and the beamforming weights are calculated with MAEPLL.

The antenna array is a calibrated multi-antenna array with known geometry and consists of A antenna elements with the antenna element $a \in \{1, \dots, A\}$ and the antenna element displacement vector \mathbf{d}_a . The antenna reference point equals the first antenna element $a = 1$. The antenna receives N satellite signals of the satellites $n, m \in \{1, \dots, N\}$, while the highest satellite is also the reference satellite for the double-differencing (DD). Each satellite transmits M signals on different frequencies with frequency slot $\mu \in \{1, \dots, M\}$, frequency f_μ and wavelength λ_μ . Each signal $s_{a;\mu}^n$ transmitted from satellite n at frequency slot μ and received at antenna element a is tracked with the receiver using a common numerical controlled oscillator (NCO). Due to the slaved tracking all received signals have a common base for the carrier ambiguities. The code pseudorange and the carrier phase pseudorange are calculated for all signals, at all antenna elements. The DDPC is defined by

$$\nabla \Delta P_{a,b;\mu}^{n,m} = \Delta P_{a,b;\mu}^m \overline{\Delta P_{a,b;\mu}^n} = P_{a;\mu}^m \overline{P_{b;\mu}^m} \overline{P_{a;\mu}^n} P_{b;\mu}^n = \alpha_{a;\mu}^m \alpha_{b;\mu}^m \alpha_{a;\mu}^n \alpha_{b;\mu}^n \exp\left\{j \frac{2\pi}{\lambda_\mu} \nabla \Delta \phi_{a,b;\mu}^{n,m}\right\} \quad (1)$$

with the prompt correlator

$$P_{a;\mu}^m = \sqrt{2 \frac{C_{a;\mu}^m}{N_0} B T_{coh}} \exp\left\{j \frac{2\pi}{\lambda_\mu} \phi_{a;\mu}^m\right\} = \alpha_{a;\mu}^m \exp\left\{j \frac{2\pi}{\lambda_\mu} \phi_{a;\mu}^m\right\} \quad (2)$$

and the double differenced phase

$$\nabla \Delta \phi_{a,b;\mu}^{m,n} = \phi_{a;\mu}^m - \phi_{b;\mu}^m - \phi_{a;\mu}^n + \phi_{b;\mu}^n \quad (3)$$

In the equations above the antenna index a represents the reference antenna element and the satellite index n the satellite reference index. The amplitudes $\alpha_{a;\mu}^m$ in Eq. (1) are real-valued, $\nabla \Delta P_{a,b;\mu}^{n,m}$ is complex and \overline{P} represents the complex conjugated. Considering not only one LOS but also P MP signals and expressing the phase offset with respect to the reference antenna element and geometrical considerations (see Figure 3, left), the prompt correlator value of Eq. (2) can be approximated by

$$P_{a;\mu}^m \approx \sum_p \alpha_p^m \exp \left(j \mathbf{k}_{\mu;p}^m \cdot \mathbf{d}_a + j \frac{2\pi}{\lambda_\mu} \phi_{1;\mu;p}^m \right), \quad (4)$$

with p representing the signal index (0 ... line-of-sight; 1, 2, ... multipath), α_p^m the signal amplitude and \mathbf{k}_p^m the angular wave number ($\mathbf{k}_{p=0}^m$ proportional to unit-vector in direction to satellite m). The parameter $\mathbf{k}_{\mu;p}^m$ is a function of the elevation and azimuth of the DOA $\mathbf{k}_{\mu;p}^m(\theta^m, \Phi^m)$. For the LOS signals, elevation and azimuth can be derived from the platform attitude. For the MP signal, azimuth and elevation need to be estimated directly. The DOA can be expressed in the antenna reference frame (ARF) or in the ENU frame. $\phi_{1;\mu;p}^m$ equals the phase of the wave front p at antenna element 1. (see Figure 3).

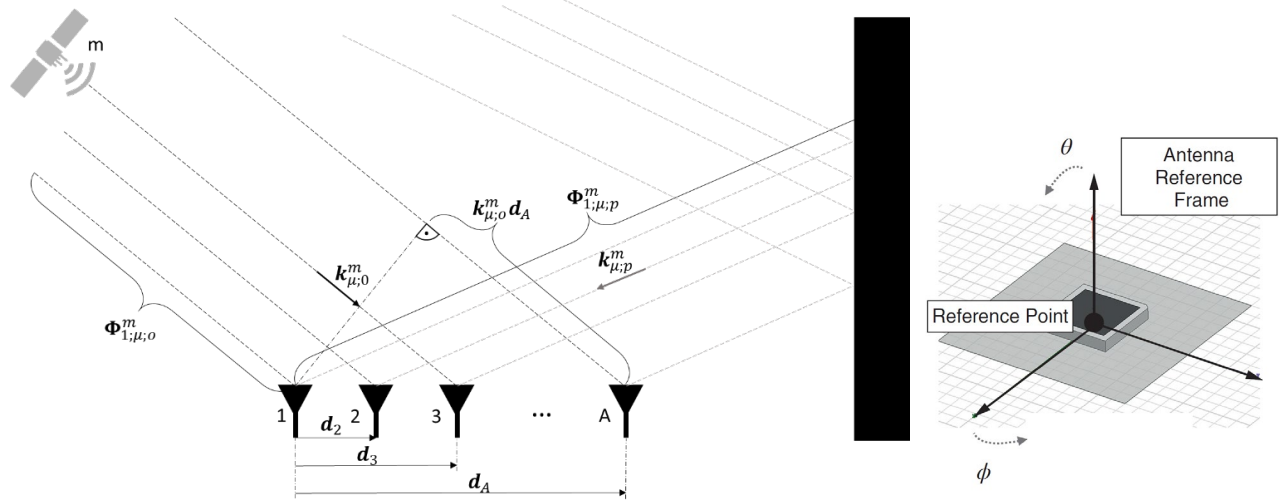


Figure 3: Relation of phase measurements with multipath at an antenna array (left) and its reference frame (right).

Equation (4) states that the effectively impinging electromagnetic wave at antenna element a is the superposition of the LOS and the multipath waves, each with a different amplitude and the phase being defined in relation to the phase of the respective signal phase at antenna element 1.

It is also assumed, the received amplitude is independent from the antenna elements a, b and the carrier index μ . With this assumption the double differenced prompt correlator can be modeled as

$$\nabla \Delta P_{a,b;\mu}^{m,n} \approx \sum_P \sum_Q \sum_R \sum_S \alpha_p^m \alpha_q^m \alpha_r^n \alpha_s^n \exp j [\mathbf{k}_{\mu;p}^m \cdot \mathbf{d}_a - \mathbf{k}_{\mu;q}^m \cdot \mathbf{d}_b - \mathbf{k}_{\mu;r}^n \cdot \mathbf{d}_a + \mathbf{k}_{\mu;s}^n \cdot \mathbf{d}_b], \quad (5)$$

with P, Q, R and S as signal indexes of the four prompt correlator values forming the DDPC. The equation represents a relation between double-differenced prompt correlator values, the attitude of the antenna platform, the wave vectors of potentially present multipath signals and the signal amplitudes. If only the line-of-sight signal is present ($P=Q=R=S=0$), it reduces to

$$\nabla \Delta P_{a,b;\mu}^{m,n} \approx \alpha_0^m \alpha_0^m \alpha_0^n \alpha_0^n \exp j [\mathbf{k}_{0;\mu}^m \cdot (\mathbf{d}_a - \mathbf{d}_b) - \mathbf{k}_{0;\mu}^n \cdot (\mathbf{d}_a - \mathbf{d}_b)] \quad (6)$$

If one MP signal for each LOS signal is present ($P=Q=R=S=1$), it becomes

$$\begin{aligned}
& \nabla \Delta P_{a,b;\mu}^{m,n} \\
& \approx [\alpha_{\mu;0}^m]^2 \exp\{i \mathbf{k}_{\mu;0}^m \mathbf{d}_b\} \\
& + \alpha_{\mu;0}^m \alpha_{\mu;1}^m \exp\{i(|\mathbf{k}_{\mu}^m| \Delta L_{1;01}^m + \mathbf{k}_{\mu;1}^m \mathbf{d}_b)\} \\
& + \alpha_{\mu;1}^m \alpha_{\mu;0}^m \exp\{i(-|\mathbf{k}_{\mu}^m| \Delta L_{1;01}^m + \mathbf{k}_{\mu;0}^m \mathbf{d}_b)\} \\
& + \alpha_{\mu;1}^m]^2 \exp\{i \mathbf{k}_{\mu;1}^m \mathbf{d}_b\} \\
& * [\alpha_{\mu;0}^n]^2 \exp\{-i \mathbf{k}_{\mu;0}^n \mathbf{d}_b\} \\
& + \alpha_{\mu;0}^n \alpha_{\mu;1}^n \exp\{-i(|\mathbf{k}_{\mu}^n| \Delta L_{1;01}^n + \mathbf{k}_{\mu;1}^n \mathbf{d}_b)\} \\
& + \alpha_{\mu;1}^n \alpha_{\mu;0}^n \exp\{-i(-|\mathbf{k}_{\mu}^n| \Delta L_{1;01}^n + \mathbf{k}_{\mu;0}^n \mathbf{d}_b)\} \\
& + \alpha_{\mu;1}^n]^2 \exp\{-i \mathbf{k}_{\mu;1}^n \mathbf{d}_b\},
\end{aligned} \tag{7}$$

with the assumptions $\alpha_{a;\mu;p}^m = \alpha_{b;\mu;p}^m = \alpha_{\mu;p}^m$, $\mathbf{d}_a = [0 \ 0 \ 0]^T$, $\phi_{1;\mu;0}^m - \phi_{1;\mu;1}^m = \Delta\phi_{1;\mu;01}^m$ and $\exp\{\Delta\phi_{1;\mu;01}^m\} = \exp\left\{\Delta L_{1;01}^m * \frac{2\pi}{\lambda_\mu}\right\} = \exp\{|\mathbf{k}_{\mu}^m| \Delta L_{1;01}^m\}$. Where $\Delta L_{1;01}^m$ represents a geometrical distance or delay between the LOS and the MP signal at the reference antenna element. The vector of unknowns in Eq. (6) is

$$x = [\text{Yaw Roll Pitch } \alpha_0^{1xN}] \tag{8}$$

and for Eq. (7)

$$x = [\text{Yaw Roll Pitch } \alpha_0^{1xN} \ \alpha_1^{1xN} \ \theta_1^{1xN} \ \Phi_1^{1xN} \ \Delta L_{1;01}^{1xNP}], \tag{9}$$

with the unknown parameters:

- Platform attitude (Yaw Roll Pitch) (3 parameter)
- LOS amplitudes α_0^{1xN} (N parameter)
- MP
 - Amplitudes α_1^{1xN} (N parameter),
 - Elevation θ_1^{1xN} (N parameter),
 - Azimuth Φ_1^{1xN} (N parameter) and
 - delay LOS-MP $\Delta L_{1;01}^{1xNP}$ (N parameter).

For the system considered here, for each coherent integration interval a number of $M(A-1)(N-1)$ complex DDPC values are obtained, representing $2M(A-1)(N-1)$ real valued observations. The condition to solve the unknown parameters is

$$2M(A-1)(N-1) \geq 3 + N + 4NP. \tag{10}$$

Another possibility to set up the DDPC model is to extend the antenna element displacement vectors \mathbf{d}_a with a phase center correction (PCC) term. The PCC is composed of the phase center offset (PCO) and the phase center variation (PCV). The elevation and azimuth dependent $PCC_a(\theta, \varphi)$ of antenna element a can be modeled by a series of spherical harmonics $Y_l^m(\theta, \varphi)$. Eq. (6) reads

$$\nabla \Delta P_{a,b;\mu}^{m,n}(x) \approx \alpha_{a;\mu}^m \alpha_{b;\mu}^m \alpha_{a;\mu}^n \alpha_{b;\mu}^n \exp\{j [\mathbf{k}_{0;\mu}^m \cdot ((\mathbf{d}_a + PCC_a) - \mathbf{d}_b(PCC_b)) - \mathbf{k}_{0;\mu}^n \cdot ((\mathbf{d}_a + PCC_a) - (\mathbf{d}_b + PCC_b))]\} \tag{11}$$

with a vector of unknowns equals

$$x = [\text{Yaw Roll Pitch } \alpha_0^{1xN} \ A_{uv}^{1xAxU} \ B_{uv}^{1xAxU}]. \tag{12}$$

A_{uv}^{1xAxU} and B_{uv}^{1xAxU} are the coefficients of the spherical harmonics and U indicates the number of the coefficients.

SIMULATION

The baseline for the simulations is a multi-GNSS constellation including the GPS, Galileo and Beidou satellites with a total of 84 satellites. Furthermore, a variety of scenarios is simulated including open sky conditions with and without ground multipath, as well as varying thermal AWGN, additional frequencies, different initial guess errors and two antenna element gain patterns. Changing the listed parameter of the simulation allows to study the performance and the behavior of the MAEPLL core algorithm.

The simulation framework is a MATLAB based channel impulse response (CIR) simulation tool. The incoming GNSS signals are simulated for each antenna element. The constellation, the antenna array, the scenario and the multipath environment is setup and simulated.

In the MAPELL core module the complex prompt correlator values are derived from the incoming wave fronts (LOS plus MP). Signal power (C/N_0), the phase of LOS and all MP signals are considered, as well as the antenna gain pattern for co- and cross-polarization. With the prompt correlator values for each satellite and each antenna element, the DDPC values are calculated. To form the DDPC, the first antenna element is chosen as reference antenna element and the highest satellite as reference satellite. The model for the DDPC values from Eq. (6) or (7) is setup and used in a non-linear least squares estimation process, expressed as

$$\min_x \sum_{\mu} (\nabla \Delta P_{\text{model}}(x, \mu) - \nabla \Delta P_{\text{observation}, \mu})^2, \quad (13)$$

with x representing the state to estimate from Eq. (8) (No MP estimation) or (9) (with MP estimation). $\nabla \Delta P_{\text{model}}$ represents the DDPC values derived from the models presented in Eq. (6) and (7), $\nabla \Delta P_{\text{observation}, \mu}$ represents the DDPC values coming from the observations in particular from a real measurement or like in this case from a simulation. The MATLAB function *lsqcurvefit* is used with an initial state of $x = x_0$ and lower and upper bound limits. The estimated state for the attitude, the LOS amplitude and the MP DOA, amplitude and the phase delay is then compared with the true state. The error between estimated and true attitude is evaluated for several runs and the variance of the accuracy of the estimated attitude is calculation. This is done for the defined scenarios and cases. Eq. (13) uses no additional weighting scheme, however, as the signal amplitudes are considered in the $\nabla \Delta P$ terms, the stronger the signal the stronger it contributes to the residual.

Two antenna gain patterns were used, where the first one is an isotropic gain pattern with 0 dBi in all directions for RHCP and LHCP signals. The isotropic gain pattern is illustrated in Figure 4. The second studied gain pattern represents a common GNSS antenna. The simulated gain pattern of the Comrod GNSS-MILANT antenna [9] is used and plotted in Figure 5.

A standard uniform rectangular array (URA) geometry with four antenna elements with an element spacing of $\frac{\lambda}{2}$ at L1 frequency is set. A GPS C/A like ranging signal on the L1 frequency and a receiver processing with 10MHz receiver frontend bandwidth and 10ms coherent integrations time is assumed.

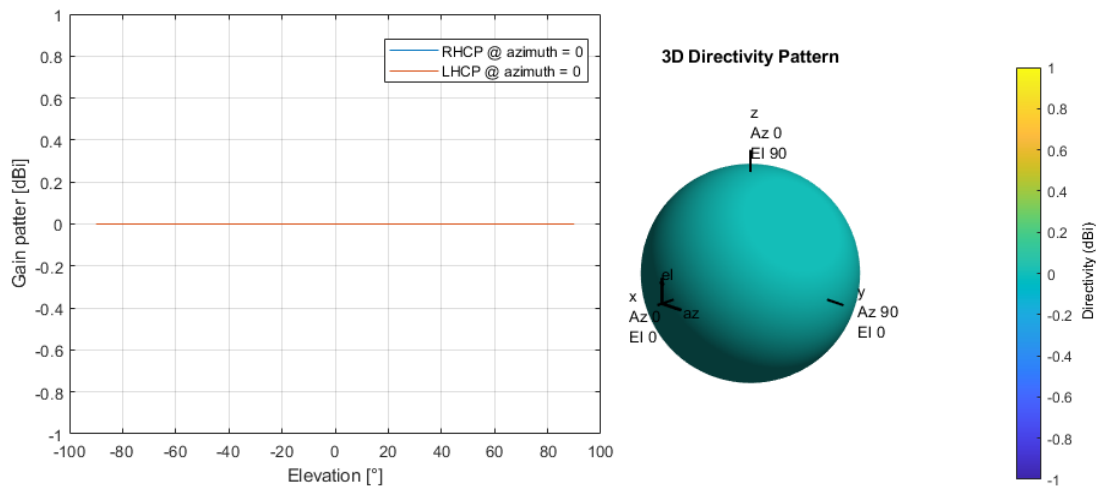


Figure 4: Gain pattern of isotropic antenna element.

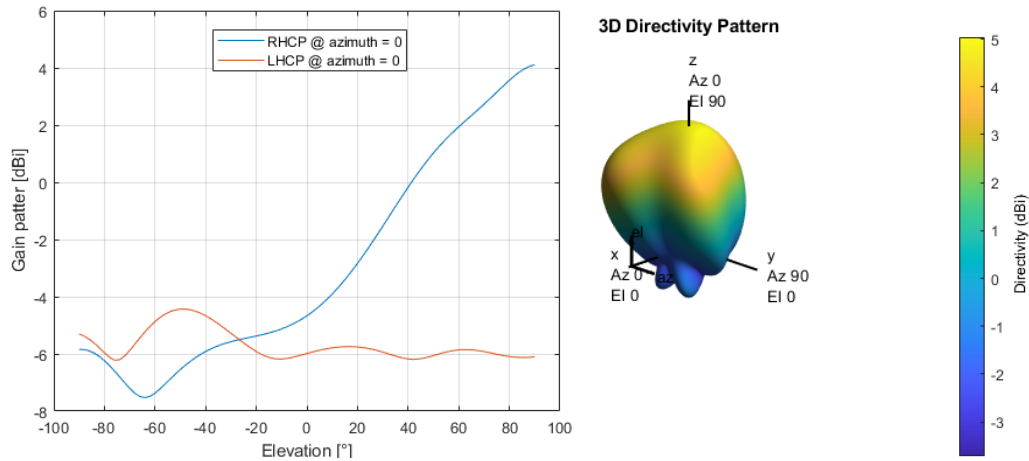


Figure 5: Simulated gain pattern of the Comrod GNSS-MILANT [9] antenna.

RESULTS

The result section is divided into seven subsections:

1. Verification of DDPC model
2. Influence of C/N_0
3. Influence of initial guess error
4. Influence of second frequency
5. Influence of antenna pattern
6. Attitude with MP DOA estimation and second frequency
7. Influence of MP parameter starting conditions

In the first section, the general validity of the derived mathematical DDPC model is verified. In section 2, 3, 4 and 5 the influence of signal power, erroneous initial assumptions on the attitude, second frequency and the antenna pattern are analyzed by changing only the respective parameter. In section 2-5 no MP components are present in the observations of the simulation and MAEPLL uses the DDPC model of Eq. (6) where only the attitude and LOS amplitude is modeled and estimated. In the sections 6 and 7 ground MP components are present in the simulation measurements and the DDPC model of Eq. (7) is used to estimate attitude and MP DOA.

Verification of DDPC model

For the validation of the coherence between the simulation observations and the derived DDPC model the isotropic gain pattern is used. To remove the influence of the AWGN, the LOS C/N_0 at the 0 dBi antenna is set to 100 dB-Hz. The initial guess of the state vector $x_0 = [Yaw \ Roll \ Pitch \ \alpha_{LOS}^{1 \times N}]$ is set to the true values, in this case $x_0 = [100^\circ, 0^\circ, 0^\circ, \sqrt{2}, \dots, \sqrt{2}]$. In the next step, the Double-Differenced Prompt Correlator values of the simulation are compared to the DDPC values coming from the model, see Eq. (6). In Figure 6 (left) the complex DDPC values are plotted. In total, there are $(27 - 1)(4 - 1)\mathbf{1} = 78$ complex DDPC values coming from 27 satellites, 4 antenna elements and 1 frequency. The black circles represent the DDPC observations of the simulation ($\nabla \Delta P_{\text{observation}}$) in the complex plane and the red crosses represent the DDPC values derived from the model in Eq. (6) ($\nabla \Delta P_{\text{model}}$) and the state vector $x_0 = [100^\circ, 0^\circ, 0^\circ, \sqrt{2}, \dots, \sqrt{2}]$ containing the true values. It can be observed, that the DDPC values of the observations and the model fit perfectly. This validates the model for the simplest case when no MP is neither present, nor estimated. It can also be seen, that the DDPC values line up on a circle, because of the signal power of 1 (amplitude equals $\sqrt{2}$) for each signal and the isotropic antenna with 0dB gain in all directions. The value of 4 comes from the factors $\alpha_0^m \alpha_0^m \alpha_0^n \alpha_0^n$ of Eq. (6) where all $\alpha_0 = \sqrt{2}$ resulting in $\sqrt{2}^4 = 4$.

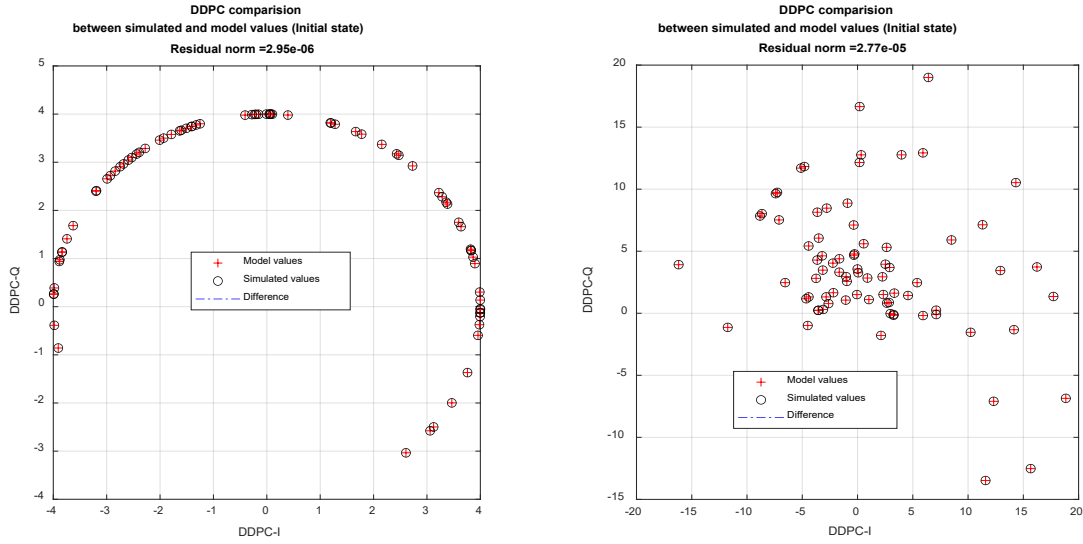


Figure 6: 78 Double-Differenced-Prompt-Correlator (DDPC) values of simulation and of the DDPC model. Left: Only LOS signals are simulated and modeled. Right: LOS and ground multipath. 78 DDPC values coming from 27 satellites, 4 antenna elements and 1 frequency $(27 - 1)(4 - 1)1 = 78$.

The DDPC model with one multipath component per satellite signal, Eq. (7), is evaluated in the same manner. But now the ground reflections are considered during the simulation. LOS and the ground multipath signals are present in the observations. The strong C/N_0 is still at 100dB-Hz and the initial attitude error is also at 0 as before. The initial errors for the MP estimation, namely amplitude error $\delta\alpha_1$, Azimuth error $\delta\Phi_1$, Elevation error $\delta\theta_1$ and Delay error $\delta\Delta L^{1xNP}$ are set to zero as well to have the true state vector x_0 .

In Figure 6 (right) the DDPC values are plotted in the complex plane for the observed and the modeled DDPC values. Again, the 78 DDPC values of the model for Eq. (7) match perfectly the observations of the simulation, when the state vector $x_0 = [Yaw \ Roll \ Pitch \ \alpha_0^{1xN} \ \alpha_1^{1xN} \ \theta_1^{1xN} \ \Phi_1^{1xN} \ \Delta L_{1;01}^{1xNP}]$ is initialized with the true values for the attitude, the LOS amplitude and the MP parameter. The DDPC values are not anymore on a circle as the strong ground multipath components interfere with the LOS signal and reduces or increases the combined signal power.

The geometrical DDPC model is correct and matches the DDPC observations derived from the simulation, when all the state parameters are identical to the true simulated values.

In the following sections, the difference of simulated DDPC observations ($\nabla\Delta P_{\text{observation}}$) and the values derived from the DDPC model ($\nabla\Delta P_{\text{model}}$), namely the residual norm (Eq. (13)), are used to optimize the state parameters in a LSQ optimization process.

Influence of C/N_0

In this section the influence of the signal strength C/N_0 is evaluated. The estimated attitude accuracy is evaluated for weak signals with 35dB-Hz and compared to strong signals with 55dB-Hz. The initial attitude error is $[5^\circ \ 2^\circ \ 2^\circ]$ in yaw, roll and pitch the initial LOS amplitude is the true value of 1. In Figure 7, Figure 8 and Figure 9 the results of the attitude estimation process are illustrated for a C/N_0 of 55dB-Hz. In Figure 10 and Figure 11 the results are displayed for a C/N_0 of 35dB-Hz. Figure 7 and Figure 10 show the DDPC values before and after the LSQ optimization. Figure 8 shows the residuum norm and the convergence of the LSQ optimization. Figure 9 and Figure 11 show the attitude and LOS amplitude of the estimation process before and after the LSQ optimization and are subdivided into an azimuth and elevation error plot in the top row and a LOS signal power plot at the bottom row. The attitude error for 55 dB-Hz is $[0.04^\circ \ -0.46^\circ \ -0.22^\circ]$ in yaw, roll and pitch compared to an attitude error of $[0.40^\circ \ 2.49^\circ \ -0.62^\circ]$ for 35 dBHz. The attitude can be estimated with less error for higher C/N_0 values. The reason can be seen nicely comparing the right side of Figure 7 and Figure 10. The additional noise in the 35 dB-Hz case cannot be modeled by Eq. (6) so the DDPC values of model and simulation are not matching as well as for the case of 55 dB-Hz. This also results in a higher uncertainty in the attitude estimation. The optimization algorithm tries to vary the LOS signal power and attitude to compensate for the noise influence.

For this section it can be summarized that the C/N_0 has an influence on the accuracy of the attitude estimation. But even for low C/N_0 value of 35 dB-Hz the attitude can still be estimated with an accuracy in the range of a few degrees.

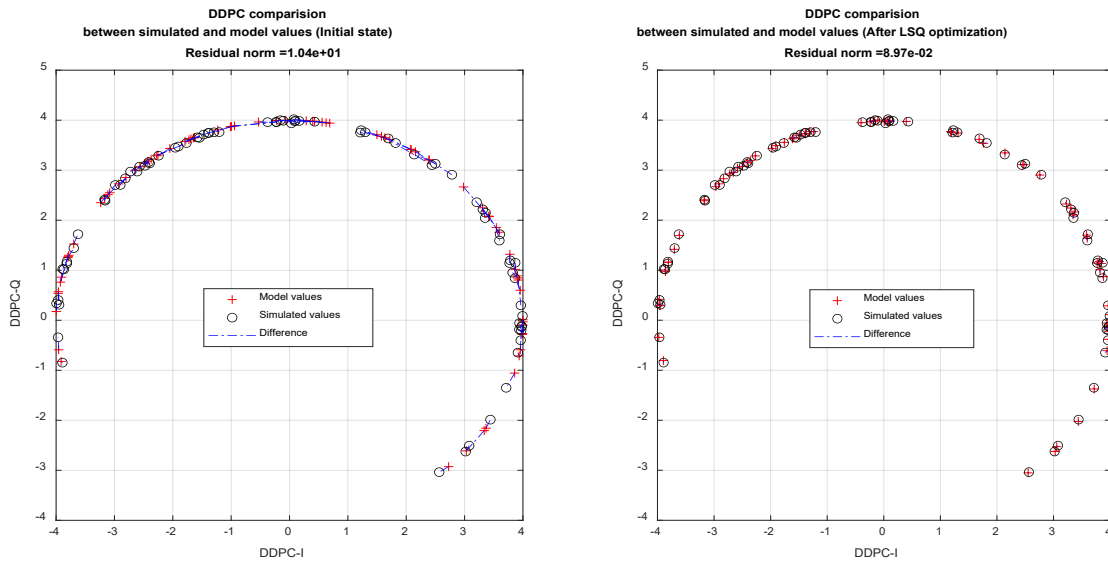


Figure 7: DDPC values of simulation and the model for LOS only with a C/No of 55 dB-Hz. Left: DDPC values with initial state parameter and an attitude error of $[5^\circ \ 2^\circ \ 2^\circ]$. Right: DDPC values after LSQ optimization. With a final residual norm of 8.97×10^{-2} after 4 optimizations steps.

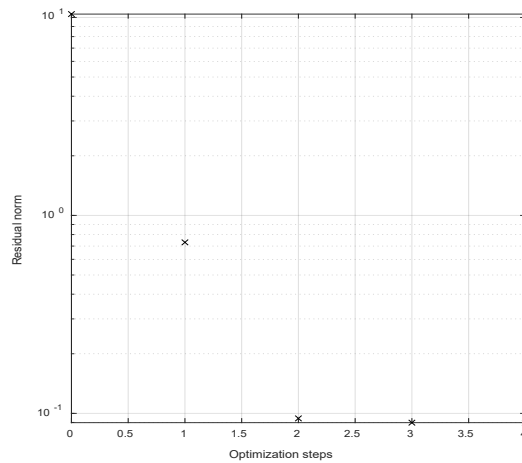


Figure 8: Residual norm of the optimization steps starting at an attitude error of $[5^\circ \ 2^\circ \ 2^\circ]$ and a C/No of 55 dB-Hz.

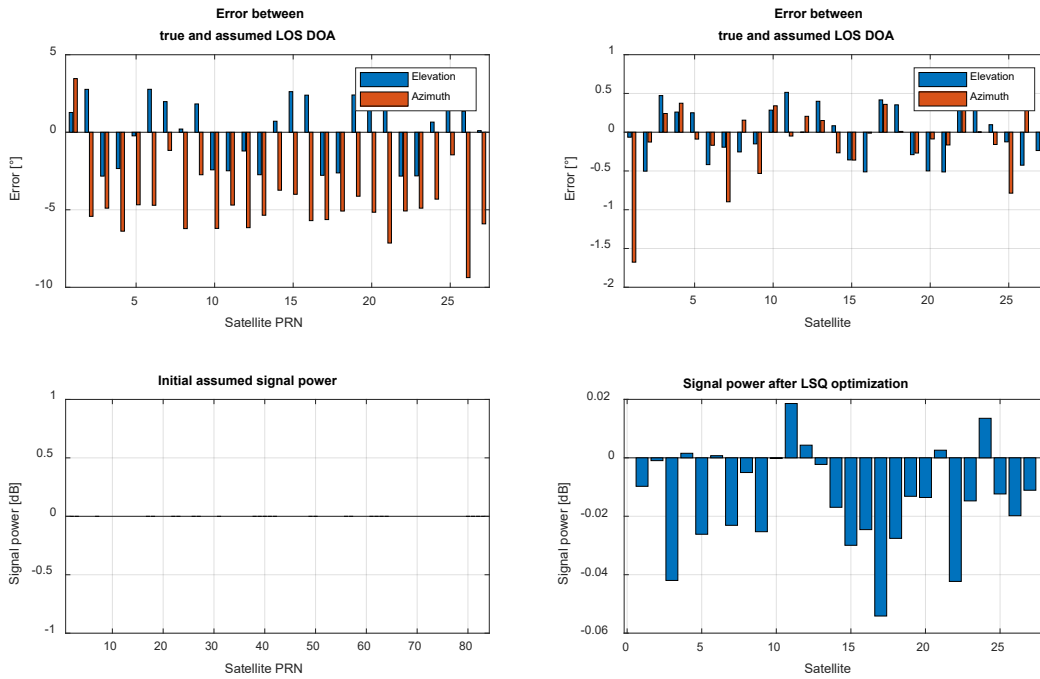


Figure 9: Visualization of the attitude estimation process with a C/N_0 of 55dB-Hz . On the left side the initial starting state condition for the LSQ optimization. On the right side the final state conditions after the LSQ optimization. Top row shows the azimuth and elevation error for true and assumed attitude. Bottom row shows the LOS signal power. The initial attitude error is $[5^\circ \ 2^\circ \ 2^\circ]$, the initial LOS amplitude error is 0. The attitude error after the LSQ optimization is $[0.0420 \ -0.4660 \ -0.2206]^\circ$

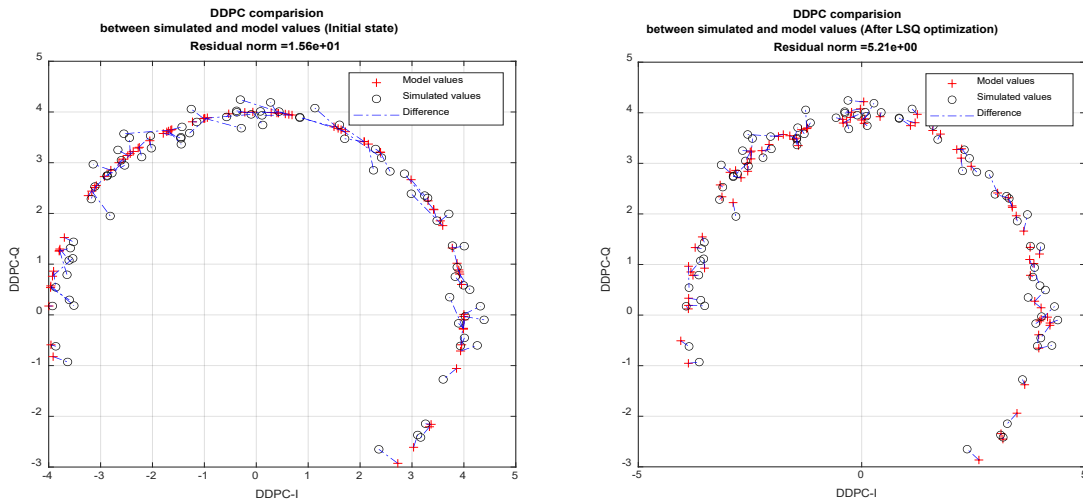


Figure 10: DDPC values of simulation and the model for LOS only with a C/N_0 of 35 dB-Hz . Left: DDPC values with initial state parameter and an attitude error of $[5^\circ \ 2^\circ \ 2^\circ]$. Right: DDPC values after LSQ optimization. With a final residual norm of 5.21 after 3 optimizations steps.

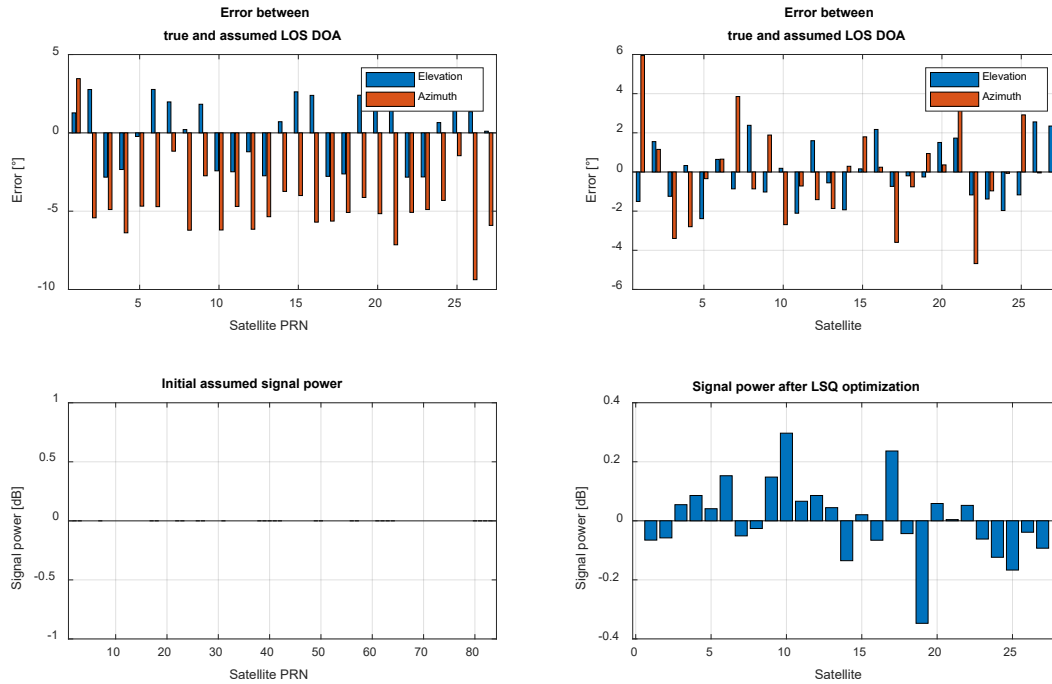


Figure 11: Visualization of the attitude estimation process with a C/N_0 of 35dB-Hz . On the left side the initial starting state condition for the LSQ optimization. On the right side the final state conditions after the LSQ optimization. Top row shows the azimuth and elevation error for true and assumed attitude. Bottom row shows the LOS signal power. The initial attitude error is $[5^\circ \ 2^\circ \ 2^\circ]$, the initial LOS amplitude error is 0. The attitude error after the LSQ optimization is $[0.4068 \ 2.4883 \ -0.6249]^\circ$.

Influence of initial guess error

A weak point in the evaluation of the section above is the calculation of the convergence of the LSQ optimization for only one specific start error configuration. Therefore, in this section a Monte Carlo simulation is performed to evaluate the influence of the initially assumed attitude error on the convergence and the final attitude error. The other scenario settings stay the same. The initially and random generated attitude error starting conditions are plotted in Figure 12 (top) for the 100 Monte Carlo simulations. The final attitude errors after the LSQ optimizations are plotted in Figure 12 (bottom). It can be seen, that even for a very high attitude error of up to 30 degrees in yaw, roll or pitch the LSQ optimization converges to the almost identical attitude and attitude error values. If only the initial attitude error is changed and anything else is kept constant, even the thermal noise contributions, it can be clearly stated that the initial attitude estimation is not critical for the convergence of the MAEPLL algorithm. More important for the final attitude error is the constellation configuration and the additional thermal noise as well as the multipath conditions as it is shown later. With this result the short coming of the model validation above, analyzing only a single attitude error starting condition, is resolved as also any other starting condition would had yielded the same final attitude error.

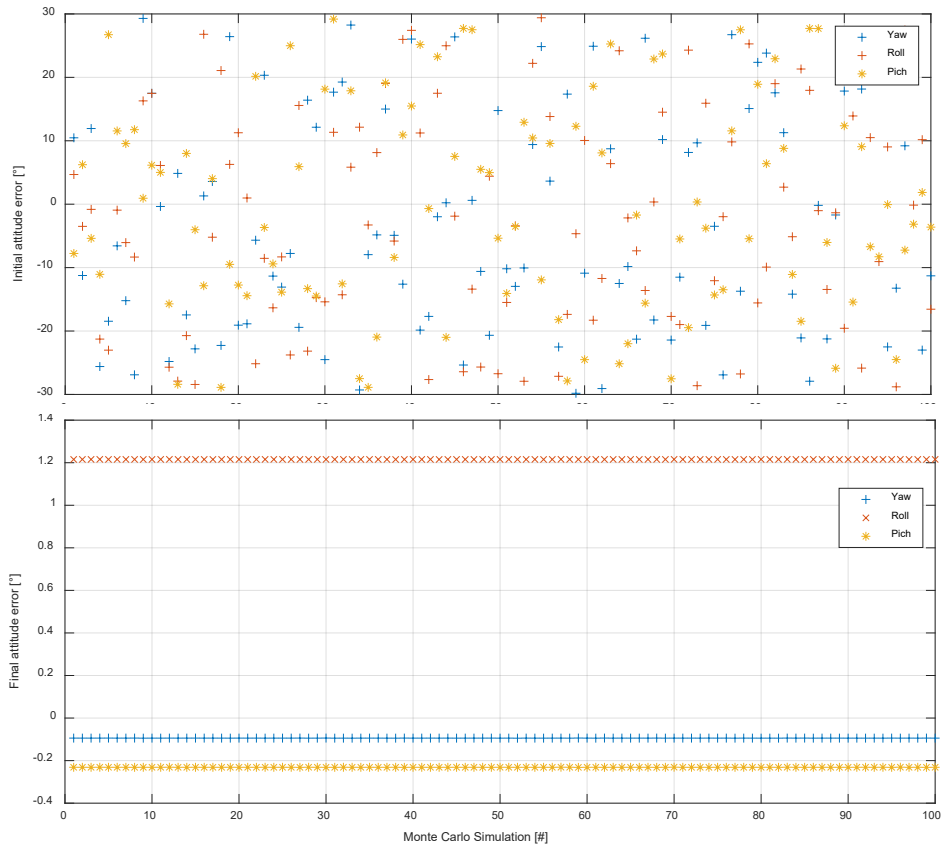


Figure 12: Initial attitude error (top) and final attitude error (bottom) after the LSQ optimization for 100 independent Monte Carlo simulations with an initial attitude error range of $\pm 30^\circ$ in yaw roll and pitch.

Influence of second frequency

The estimated attitude accuracy is compared between a single and a dual frequency scenario in the L-band. The single frequency scenario uses a signal on the L1 frequency (like in the cases above) and the dual frequency scenario uses a signal on the L1 frequency and at 3GHz. The LOS signal power C/N_0 is 45 dB-Hz. In Figure 13 the plots of the DDPC values for the single (left) and the dual frequency (right) is shown. It is obvious that the number of DDPC values double, due to the second frequency as all measurements are done also for the second carrier. Due to the different wavelength of the second carrier the additional DDPC values are not overlapping with the DDPC values of the first frequency. In Figure 14 the attitude estimation for the single (left) and the dual frequency (right) is displayed. The final attitude error of the single frequency is $[0.34^\circ -0.84^\circ -0.99^\circ]$ whereas the attitude error of the dual frequency is $[0.04^\circ 0.05^\circ -0.14^\circ]$, which is almost one order of magnitude better. To keep in mind, this is only a quantitative analysis for one single measurement. So, for one particular satellite constellation and noise environment, however, it gives a good expression of the general coherencies. It can be inferred that with a higher number of DDPC measurements it is possible to better compensate the individual noise of the DDPC measurements. The LOS signal power estimation, however, is not improved in the same manner by the second frequency.

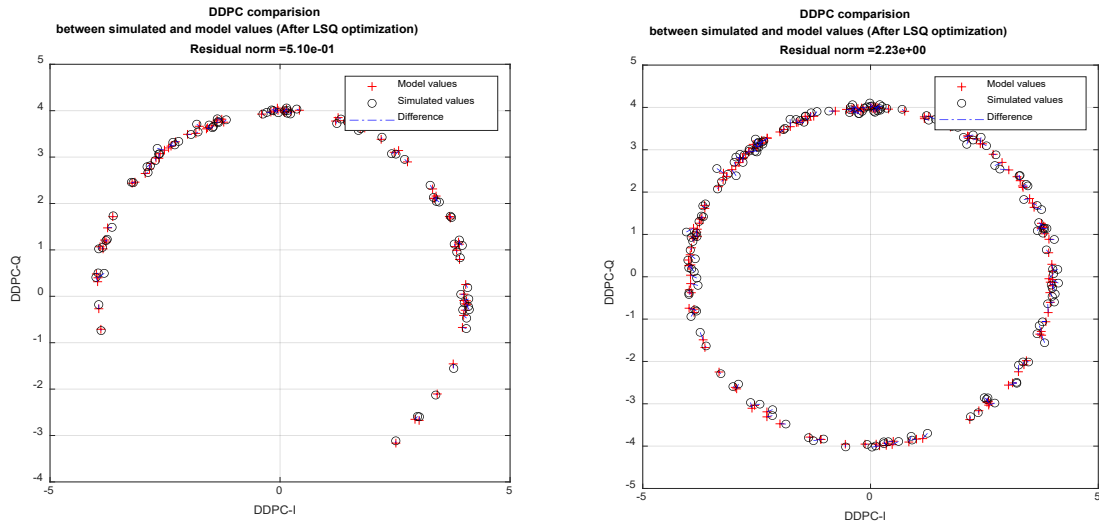


Figure 13: DDPC values in the complex plane. On the left: for a single frequency scenario with a total of 78 DDPC values. On the right: for dual frequency scenario with a total of 156 (78*2) DDPC values.

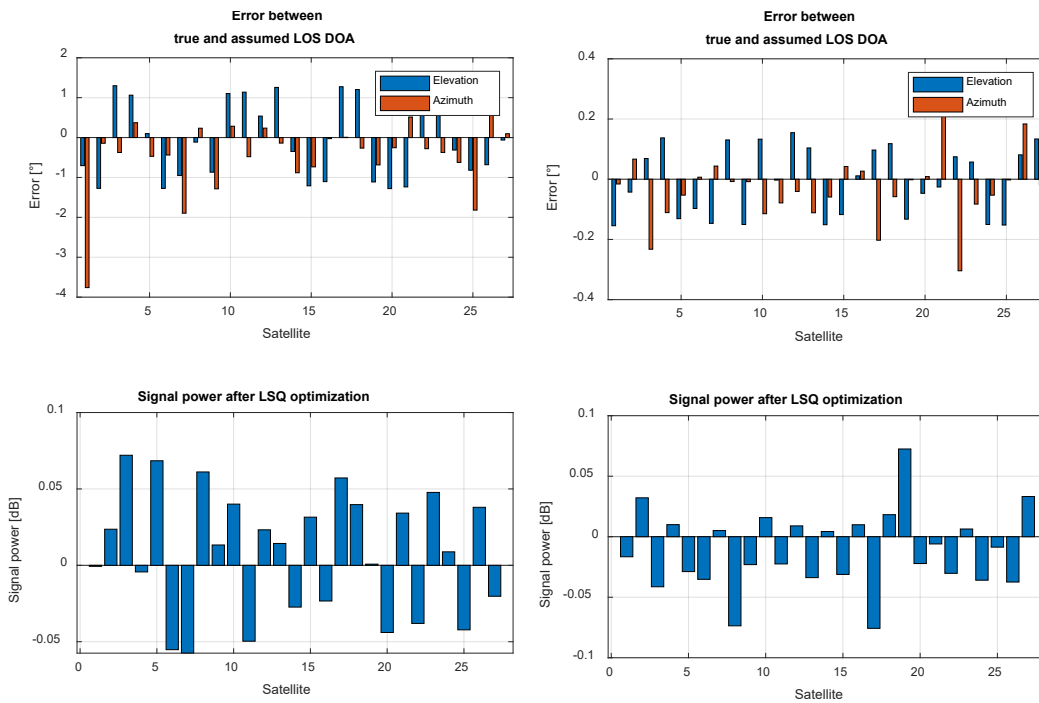


Figure 14: Visualization of the attitude estimation process with a C/N_0 of 45dB-Hz. On the left side the final state condition for **one frequency**. On the right side the final state conditions after LSQ optimization for **two frequencies**. Top row shows the azimuth and elevation error for true and assumed attitude. Bottom row shows the LOS signal power. The initial attitude error is $[5^\circ \ 2^\circ \ 2^\circ]$, the initial LOS amplitude error is 0. The attitude error after the LSQ optimization is $[0.34^\circ \ -0.84^\circ \ -0.99^\circ]$ for the single frequency and $[0.04^\circ \ 0.06^\circ \ -0.14^\circ]$ for the two frequencies.

Influence of antenna pattern

Till now, only an isotropic antenna pattern was used. It is easy to estimate the signal amplitude as no additional gain or loss is introduced by the DOA dependent antenna gain pattern. For this test the antenna gain pattern of the Comrod GNSS-Milant antenna is used. The simulated gain pattern for the LHCP and RHCP component as well as the 3D gain pattern is displayed in Figure 5. The other parameters are selected as before. Comparing the DDPC values of the initial state estimation and the final estimation after the LSQ optimization in Figure 15 shows, that the LOS signal power after the LSQ optimization is now reproducing the behavior of the antenna gain pattern. In Figure 16 (right, bottom) the LOS signal power varies between ± 5 dB and depends on the elevation of the DOA. The initial DDPC values show a big divergence of the true values in terms of the total amplitude of the DDPC values visible on the left side in Figure 15. Nevertheless, the LSQ optimization converges fast (6 optimization steps) and stable to the true DDPC values. The convergence and the good estimation of attitude and LOS amplitude can also be seen in Figure 16. It can be summarized, that the usage of a real GNSS like antenna pattern introduces an additional uncertainty for the optimization. However, this is handled stable and easily by the algorithm and does not reduce the accuracy of the attitude estimation.

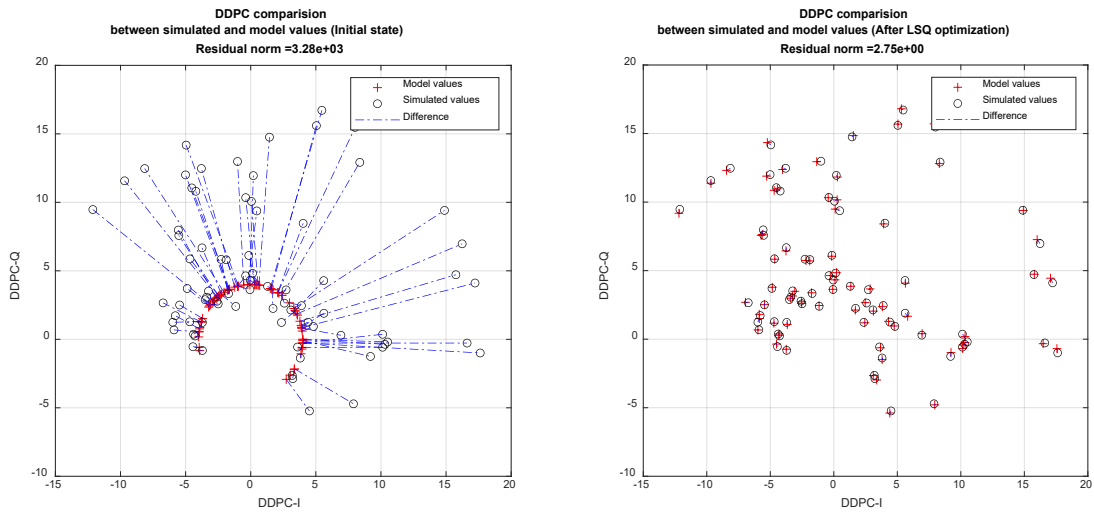


Figure 15: DDPC values of simulation and the model values for the LOS only scenario with the Comrod GNSS-Milant antenna, no MP estimation and a C/No of 45 dB-Hz. Left: DDPC values with initial state parameter and an attitude error of $[5^\circ \ 2^\circ \ 2^\circ]$. Right: DDPC values after LSQ optimization. With a final residual norm of 2.75 after 6 optimizations steps.

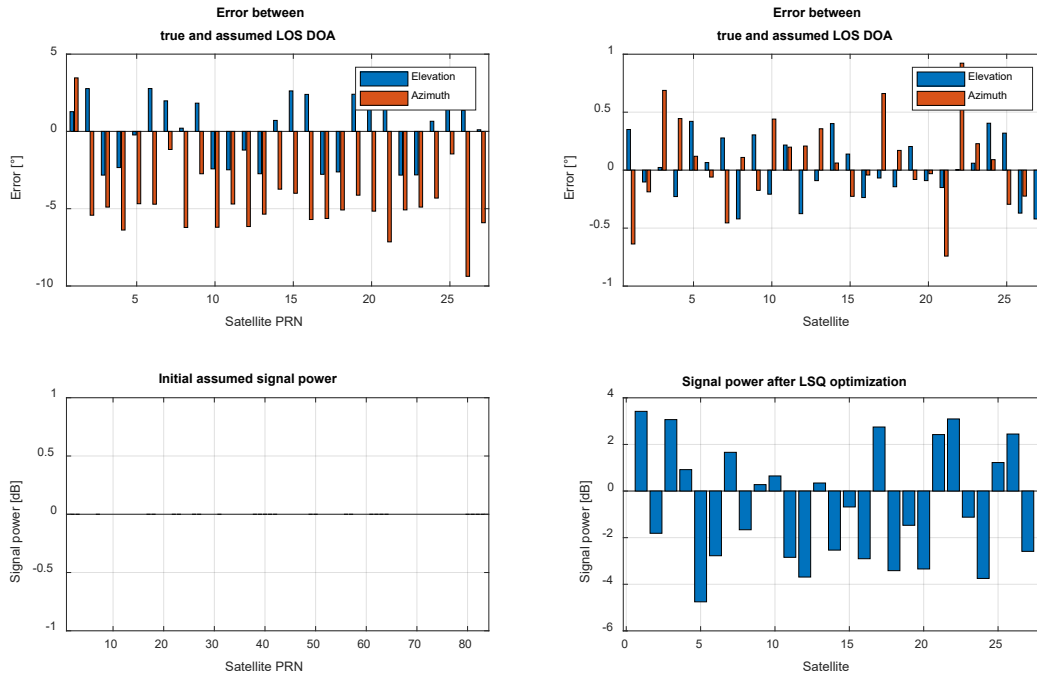


Figure 16: Visualization of the attitude estimation process with a C/N_0 of 45dB-Hz and the *Comrod GNSS-Milant* antenna. On the left side the initial starting state condition for the LSQ optimization. On the right side the final state conditions after the LSQ optimization. Top row shows the azimuth and elevation error for true and assumed attitude. Bottom row shows the LOS signal power. The initial attitude error is $[5^\circ \ 2^\circ \ 2^\circ]$, the initial LOS signal power is set to the isotropic antenna gain pattern. The attitude error after the LSQ optimization is $[-0.22^\circ \ -0.33^\circ \ -0.26^\circ]$.

Attitude with MP DOA estimation and second frequency

Only scenarios without multipath were studied so far. Now an open sky scenario with additional ground multipath signals is used for the simulation and the DDPC observations. To improve the estimation process, a second frequency is assumed, as before on L1 and 3 GHz. For simplification the isotropic antenna pattern is used with a LOS signal power of 45 dB-Hz. The MAPELL algorithm is set up to estimate array attitude, LOS amplitude, MP DOA, MP amplitude and MP delay.

In Figure 22, Figure 23 and Figure 24 the results are displayed for the case where ground MP is present and MAPELL estimates the parameters for one MP component along with the attitude and the LOS amplitudes. It can be seen in Figure 22 that the attitude estimation still works good (attitude error of $[0.35^\circ \ -0.36^\circ \ -0.61^\circ]$), even if there are strong ground MP components present. Keeping in mind, the ground MP is not damped by the antenna as an isotropic antenna pattern is used. It is also visible that the MAPELL algorithm strongly changes the LOS signal power to reduce the residual norm of the DDPC values and tries to compensate for the MP influence. The optimization convergence requires significant more optimization steps (26 optimization steps) when the MP parameter are estimated as well but the optimization converges. This indicates, that the multipath parameters are not converging as good as the attitude and LOS amplitude parameters. This can also be seen in Figure 24 where the MP parameters for the initial conditions are visualized on top. In this analysis the initial MP parameters were set to the true MP conditions. At the bottom of Figure 24 the MP parameters after the LSQ optimization are visualized and it can be seen that they are not matching the true values well after the optimization. It seems that especially the MP delay $\Delta L_{1;01}$ is a critical parameter which is not converging well. The MP delay is displayed as the phase in the right complex plane plot of Figure 24.

In the section 'Influence of C/N_0 ' the influence of the noise on the DDPC values and the attitude estimation was shown for low C/N_0 values. Now, also estimating the MP parameters, the optimization algorithm has more dimensions of freedom to compensate the random noise scattering of the DDPC values. It seems, the MP parameters are more sensitive to this noise. Higher C/N_0 values result, therefore, mainly in a better MP parameter estimation but not in a better attitude estimation.

As summary of this section, it can be stated that the additional MP estimation has increased the computational load significantly. The estimation process also converges for the MP parameter estimation but shows a significant error especially for the MP delay values $\Delta L_{1;01}$. The standard deviation of the MP DOA estimation is quite accurate with $[1.38^\circ \ 1.85^\circ]$ in azimuth and elevation but

shows to be quit challenging in other cases. The improvement due to the second frequency is mandatory for the challenging MP DOA estimation process. An open question regarding the MAEPLL estimation process is, if a second frequency below or above the L1 frequency has different impact on it.

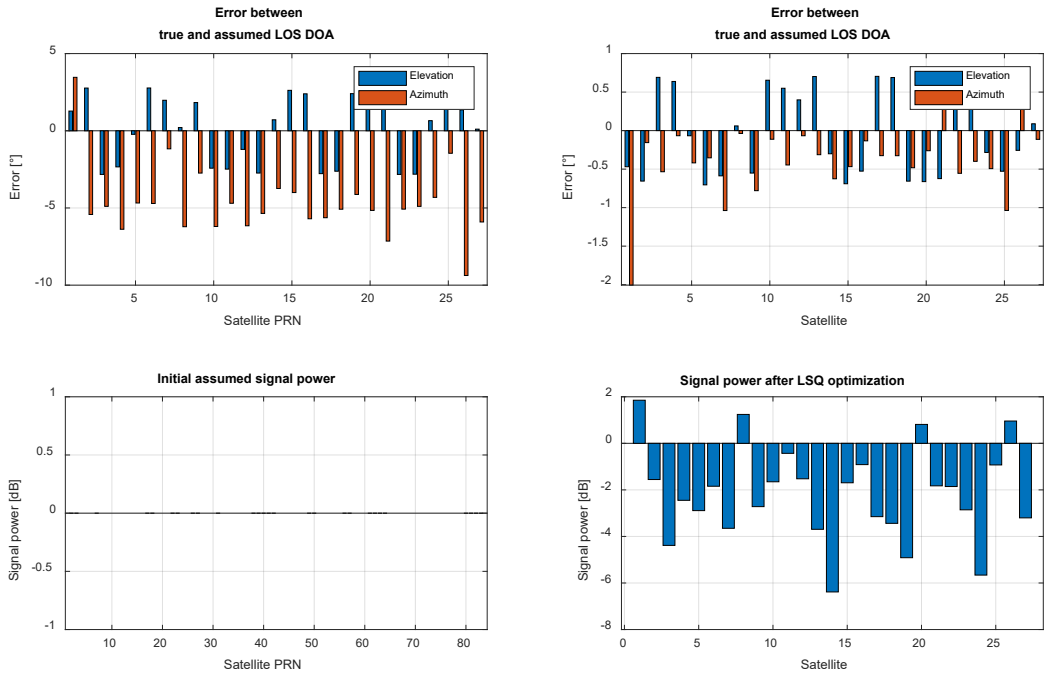


Figure 17: Visualization of the attitude estimation process with a C/No of 45dB-Hz, MP estimation and 2 frequencies. On the left side the initial starting state conditions for the LSQ optimization. On the right side the final state conditions after the LSQ optimization. Top row shows the azimuth and elevation error for true and assumed attitude. Bottom row shows the LOS signal power. The initial attitude error is $[5^\circ \ 2^\circ \ 2^\circ]$, the initial LOS amplitude error is equal to 0. The attitude error after the LSQ optimization is $[0.35^\circ \ -0.36^\circ \ -0.61^\circ]$.

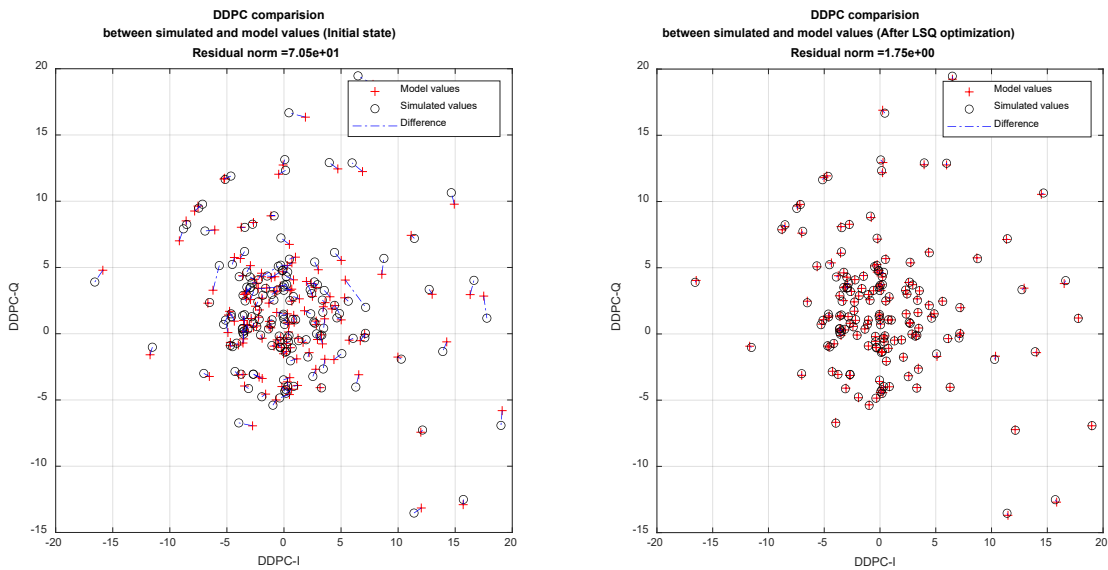


Figure 18: DDPC values of simulation and the model values for the open sky scenario with ground MP and MP estimation, 2 frequencies and with a C/No of 45 dB-Hz. Left: DDPC values with initial state parameter and an attitude error of $[5^\circ \ 2^\circ \ 2^\circ]$. Right: DDPC values after the LSQ optimization. With a final residual norm of 1.75 after 26 optimizations steps.

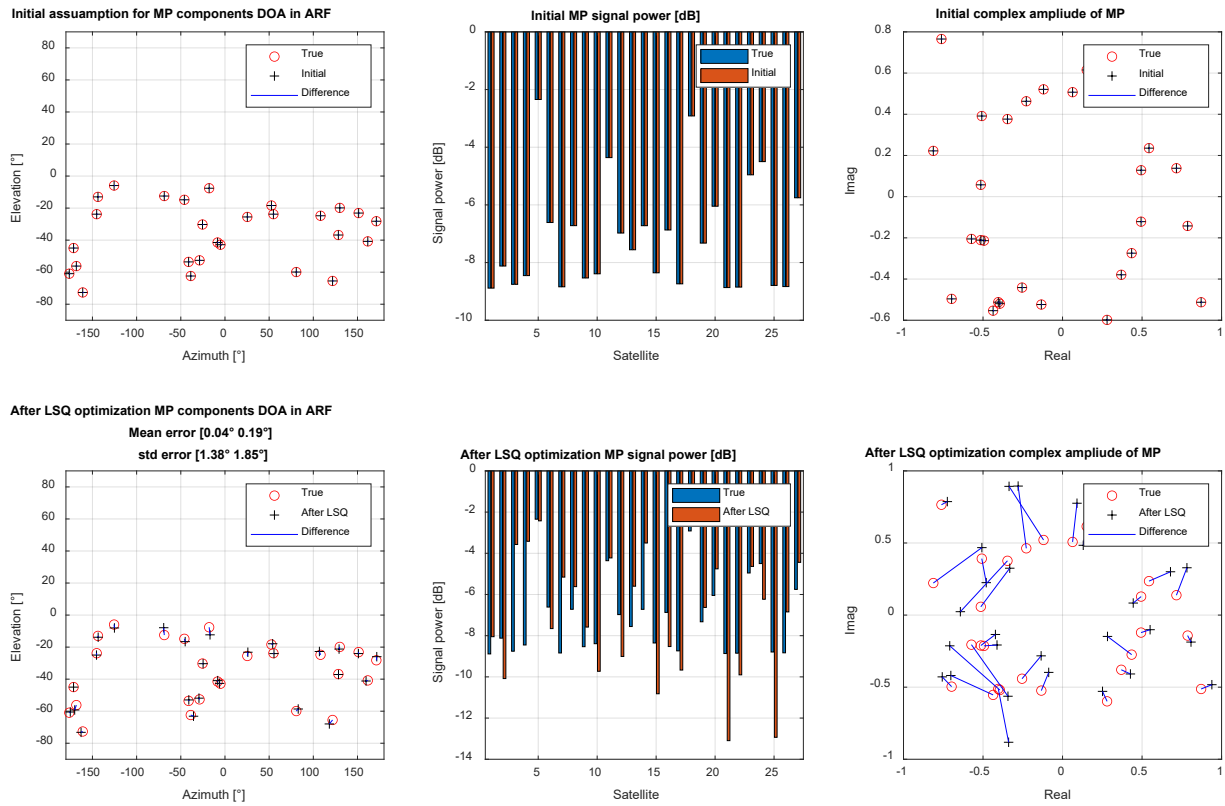


Figure 19: Visualization of the MP estimation process for 2 frequencies. Top row shows the true and initial conditions for the estimation process. Bottom row shows the true and final conditions of the LSQ optimization process. The left column is the MP DOA plot, the middle column shows the MP signal power and the right column show the complex MP signal power with ΔL as phase.

Influence of MP parameter starting conditions

In the section above the initialization of the initial MP parameters was done by the true values. In this study the influence of wrong initial MP parameter starting conditions shall be shown. Therefore, additional errors are added to the initial true MP amplitude, MP DOA in azimuth and elevation and the MP delay. The errors are random and normal distributed and defined by the standard deviation. We assume that the MAPELL algorithm is implemented in a filter, for example in an EKF where the initial starting conditions are already quite well known from the previous step. The parameters set for this evaluation are: $\sigma_{MP,\alpha} = 0.2$, $\sigma_{MP,Elevation} = 3^\circ$, $\sigma_{MP,Azimuth} = 3^\circ$ and $\sigma_{MP,Delay} = 0.01$ m. Also, the antenna gain pattern of the Comrod GNSS-Milant antenna is used.

The plots in Figure 28, Figure 29 and Figure 30 show that the additional errors introduced into the initial MP parameters reduce the accuracy of the final estimated MP parameter, whereas the attitude can still be estimated with good accuracy of $[-0.32^\circ \ 0.94^\circ \ 0.24^\circ]$. The possibility to estimate the MP parameters is reduced by using the normal GNSS antenna pattern. The gain pattern reduces the influence (power) of the MP components onto the DDPC values. In the open sky scenario all MP signals coming from negative elevation angles and are suppressed by the antenna gain pattern, therefore, they have only a reduced impact on the observed DDPC values.

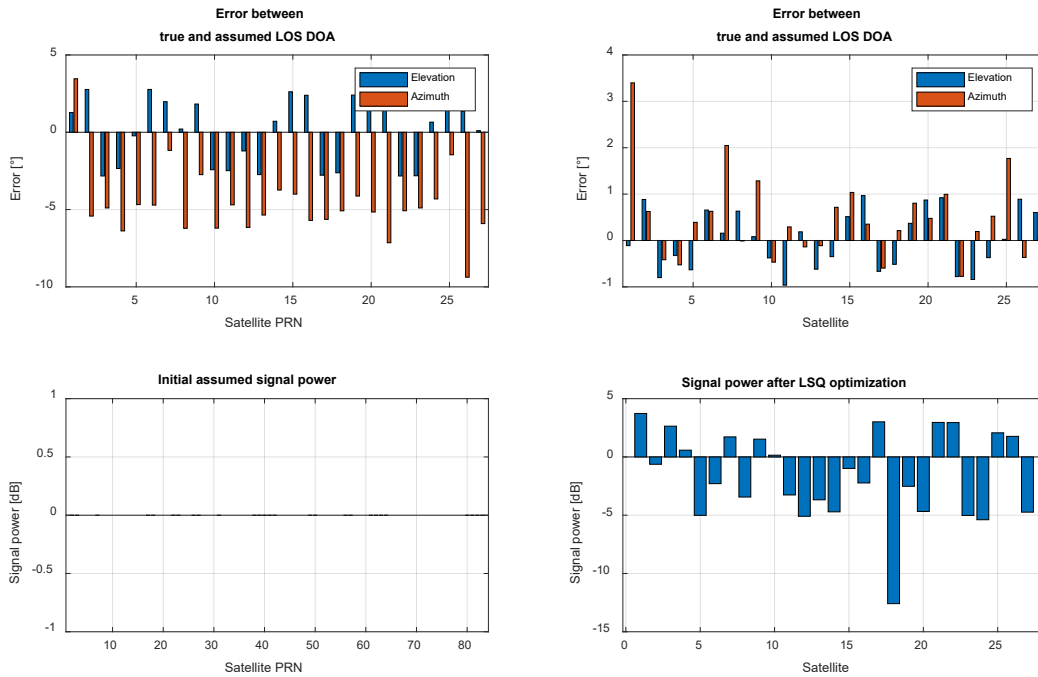


Figure 20: Visualization of the attitude estimation process with a C/N_0 of 45dB-Hz, MP estimation, 2 frequencies, Comrod GNSS-Milant antenna and with **additional initial errors on the MP parameter**. On the left side the initial starting state conditions for the LSQ optimization. On the right side the final state conditions after the LSQ optimization. Top row shows the azimuth and elevation error for true and assumed attitude. Bottom row shows the LOS signal power. The initial attitude error is $[5^\circ \ 2^\circ \ 2^\circ]$, the initial LOS amplitude error is equal to 0. The attitude error after the LSQ optimization is $[-0.32^\circ \ 0.94^\circ \ 0.24^\circ]$.

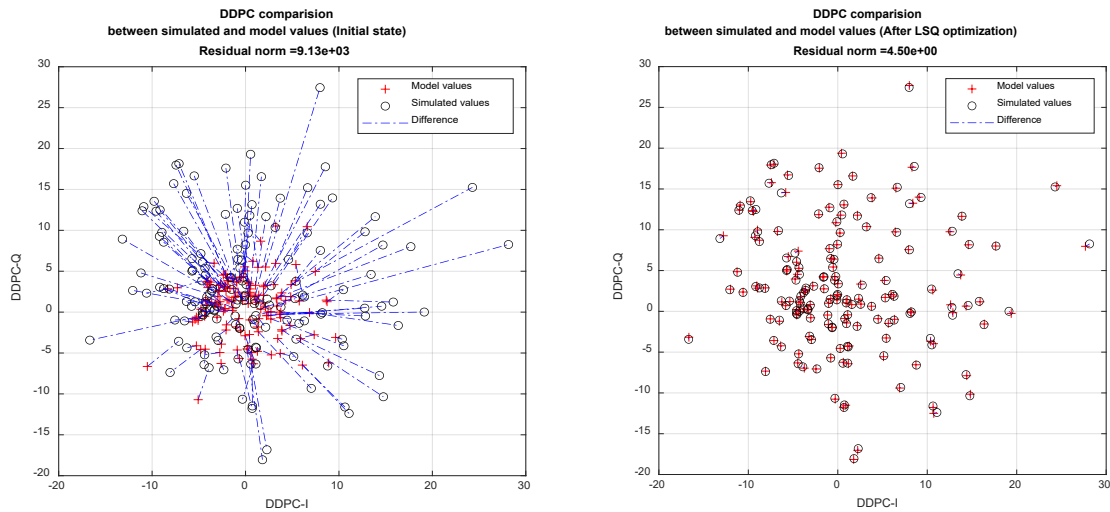


Figure 21: DDPC values of simulation and the model values for the open sky scenario with ground MP estimation, 2 frequencies, the Comrod GNSS-Milant antenna, additional initial errors on the MP parameter and with a C/No of 45 dB-Hz. Left: DDPC values with initial state parameter and an attitude error of $[5^\circ \ 2^\circ \ 2^\circ]$. Right: DDPC values after LSQ optimization. With a final residual norm of 4.5 after 26 optimizations steps.

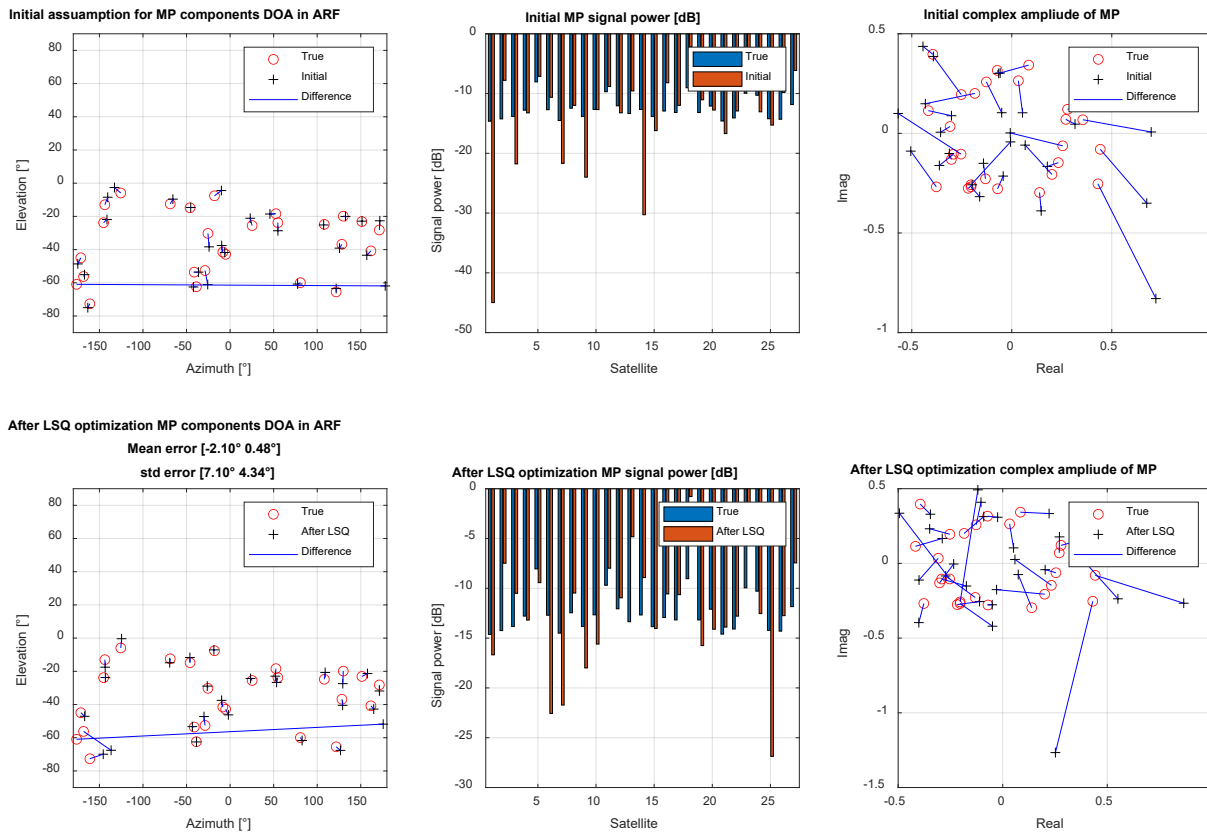


Figure 22: Visualization of the MP estimation process for 2 frequencies, the Comrod GNSS-Milant antenna and additional initial errors on the MP parameter. Top row shows the true and initial conditions for the estimation process. Bottom row shows the true and final conditions of the LSQ optimization process. The left column is the MP DOA plot, the middle column shows the MP signal power and the right column show the complex MP signal power with ΔL as phase.

SUMMARY AND OUTLOOK

A new mathematical model for the double-differenced prompt correlator (DDPC) value is presented based on the geometrical information of the antenna array. Due to the connection of the DDPC value to the attitude of the antenna array, the geometry of the antenna array and the multipath direction of arrival an easy estimation LSQ optimization process could be implemented to estimate and access these values. The post-correlation approach allows to apply non-adaptive beamforming and therefore nulling of strong MP components. The model was verified for the LOS only case and the case of LOS plus one multipath signal. The attitude estimation was performed under various scenarios changing key conditions to analyze the influence on the estimation process. The attitude estimation is very robust regarding the initially assumed attitude error as well as the MP environment and the signal power. It is shown, that the attitude accuracy is quite independent of the environmental conditions due to the double-differencing and that it is possible to jointly estimate antenna array attitude and multipath direction of arrival. The attitude accuracy is for C/N_0 values above 45 dB-Hz and 10ms coherent integration time below one degree in yaw, roll and pitch. Estimating the multipath parameter parallel to the attitude is more challenging especially the complex amplitude is difficult to estimate. This can have a significant influence on the MP DOA result. The stronger the MP signal influences the DDPC value the better the parameter can be estimated. For strong ground MP signals and an initial MP assumption of three degree standard deviation in the azimuth and elevation yield the final estimated MP DOA standard deviation to 7.10° in azimuth and 4.34° in elevation. The initial MP DOA and the final MP DOA are in the same range.

A smart selection when and which MP signal shall be estimated could bring the improvement needed for a better over all MP DOA estimation. Also, a very interesting future field of study is the integration of the estimation of phase center corrections of the antenna elements using spherical harmonics as bases, as it is done for antenna calibration methods. This would allow a on-the-fly antenna element calibration and, therefore, the usage of uncalibrated, sub-optimal and cheap antenna arrays in mass market applications.

The entire MAEPLL processing chain includes also non-adaptive beamforming with MP nulling and the improvement of code and phase measurements. The combination of the attitude and MP DOA estimation with the beamforming capabilities is the next important step to analyze the full potential of the Multipath and Attitude Estimation Phase Lock Loop.

REFERENCES

1. W.L. Stutzman, G.A. Thiele, "Antenna theory and design," *John Wiley & Sons*, 2013.
2. K. Wu et al. "An anti-jamming 5-element GPS antenna array using phase-only nulling," *ITS Telecommunications Proceedings*, 2006 6th International Conference on. IEEE, 2006.
3. M. Jaroslaw, und R. Katulski, "Detection and mitigation of GPS spoofing based on antenna array processing," *Journal of applied research and technology* 13.1 (2015): 45-57.
4. C. Fernández-Prades , J. Arribas, und P. Closas. "Robust GNSS receivers by array signal processing: theory and implementation," *Proceedings of the IEEE* 104.6 (2016): 1207-1220.
5. M. Brachvogel, et al. "A new array concept using spatially distributed subarrays for unambiguous GNSS interference mitigation in automotive applications," *Navigation* 67.1 (2020): 23-41.
6. S. Zorn, M. Niestroj, M. Meurer, F. Wendler, and M. Cuntz, "Self-contained calibration determination by jointly solving the attitude estimation and calibration problem in the steering vector domain," in *2016 8th ESA Workshop on Satellite Navigation Technologies and European Workshop on GNSS Signals and Signal Processing (NAVITEC)*, Dec 2016, pp. 1–9.
7. S. Zorn, M. Niestroj, M. Brachvogel, S. Caizzone, and M. Meurer, "Self-contained antenna crosstalk and phase offset calibration by jointly solving the attitude estimation and calibration problem," in *Proceedings of the 30th International Technical Meeting of The Satellite Division of the Institute of Navigation*, 2017.
8. S. Zorn, T. Bamberg, M. Meurer, "Accurate Position and Attitude Determination in a Jammed or Spoofed Environment Using an Uncalibrated Multi-Antenna-System," *Proceedings of the 2018 International Technical Meeting of The Institute of Navigation*, Reston, Virginia, January 2018, pp. 690-702.
9. Comrod Communication AS, "GNSS-MILANT," URL: <https://www.comrod.com/news/gnss-milant/> (Accessed: August 2021)